Integrated Guidance and Control of Moving Mass Actuated Kinetic Warheads

P. K. Menon and G. D. Sweriduk
Optimal Synthesis Inc.
4966 El Camino Real, Suite 108
Los Altos, CA 94022-1406

E. J. Ohlmeyer and D. S. Malyevac
Naval Surface Warfare Center
Code G23, 17320 Dahlgren Road
Dahlgren, VA 22448-5100

Abstract

Modeling, simulation, and integrated guidance-control of a kinetic warhead utilizing moving-mass actuators are discussed. Moving masses can be used in any speed range both in the atmosphere as well as outside it, as long as there is a force, either aerodynamic or propulsive, acting on the vehicle. Since they are contained entirely within the airframe geometric envelope, and because no mass expulsion is involved, moving-mass actuation technique offers significant advantages over conventional aerodynamic control surfaces and reaction control systems.

The present research developed a high fidelity, nine degree-of-freedom simulation model of a kinetic warhead with three moving-mass actuators. This simulation model is used for actuator sizing and in the development of flight control systems. A software package for performing numerical feedback linearization technique is employed for the design of nonlinear flight control systems. Interception of non-maneuvering and weaving targets in both atmospheric and exo-atmospheric conditions are demonstrated.

1. Introduction

Some of the earliest flight vehicles were controlled by moving the body of the pilot [1,2] to effect a change in the center of mass of the vehicle. The change in vehicle center of mass alters the flight vehicle trim, and thereby causes a change in the trajectory. Advances in aerodynamics subsequently made the moving-mass approach to flight control obsolete in all but a few, specialized applications. A present-day use of moving-mass control can be found on hang-gliders, wherein the pilot changes the relative location of his/her body with respect to the lifting plane to effect changes in flight path. Although mass movement control is no longer used on commercial flight vehicles, it continues to be important in applications such as the control of reentry vehicles at extreme Mach numbers, where the aerodynamic heating and drag penalties can make it impractical to deploy flight control surfaces.

Recently, mass movement has been proposed as a control methodology for a kinetic warhead (KW) in atmospheric and exo-atmospheric engagements [3]. As illustrated in Figure 1, the moving-mass control system changes the vehicle center of mass relative to the external forces to generate the desired control moments.

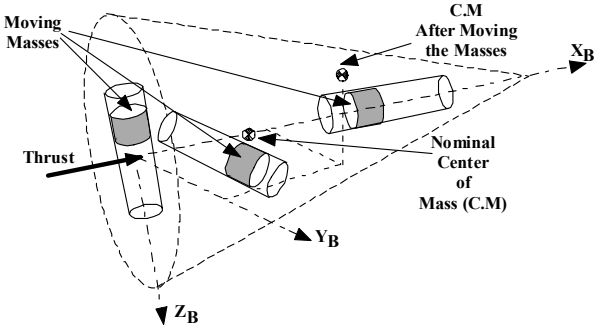

Figure 1. Moving-mass Kinetic Warhead Concept

For instance, if the thrust is aligned with the vehicle longitudinal body axis containing the nominal center of mass shown in Figure 1, moving the center of mass off the body centerline will result in thrust moments about the pitch - yaw axes. Additionally, roll

Report Documentation Page

Report Date	Report Type	Dates Covered (from... to)
29JUL2002	N/A	-

Title and Subtitle Integrated Guidance and Control of Moving Mass Actuated Kinetic Warheads	**Contract Number**
	Grant Number
	Program Element Number
Author(s)	**Project Number**
	Task Number
	Work Unit Number
Performing Organization Name(s) and Address(es) Optimal Synthesis Inc. 4966 El Camino Real, Suite 108 Los Altos, CA 94022-1406	**Performing Organization Report Number**
Sponsoring/Monitoring Agency Name(s) and Address(es)	**Sponsor/Monitor's Acronym(s)**
	Sponsor/Monitor's Report Number(s)

Distribution/Availability Statement
Approved for public release, distribution unlimited

Supplementary Notes
See Also ADM201460. Papers from Unclassified Proceedings from the 11th Annual AIAA/MDA Technology Conference held 29 July - 2 August 2002 in Monterey, CA.

Abstract

Subject Terms

Report Classification unclassified	**Classification of this page** unclassified
Classification of Abstract unclassified	**Limitation of Abstract** UU

Number of Pages
16

moments will be generated if the thrust or drag has an angular misalignment with respect to the longitudinal axis, or if the vehicle is subject to an aerodynamic lift force. The moving-mass control concept works equally well in space when the KW is thrusting, or in the atmosphere, when the vehicle experiences aerodynamic forces. Thus, this actuation technology can be employed in kinetic warheads that have both atmospheric and exo- atmospheric interception capabilities.

While the design of flight control systems using moving-mass actuation appears to be conceptually straightforward, difficulties arise due to the highly coupled and nonlinear nature of the system dynamics. This is partly due to the fact that in addition to causing changes in the vehicle center of mass, the moving-mass control system will exert inertial forces on the airframe. Moreover, the moving masses will change the instantaneous moments of inertia of the flight vehicle, which will then contribute to changes in the dynamic response. The KW control system design must deliver the desired interception accuracy while accommodating these dynamic effects.

Previous research has demonstrated that integrated design of guidance-autopilot systems can deliver fast-responding flight control systems by exploiting the synergism existing between the vehicle attitude dynamics and the translational dynamics. Recently, integrated design techniques have been investigated in the context of guidance-autopilot-fuze-warhead system design for ship-defense missiles [4, 5]. Three distinct methodologies were developed and results were obtained for the state dependent Riccati equation technique [6 – 8] and the feedback linearization approach [9 – 13]. The research discussed in References 4 and 5 were primarily motivated by the advancements in missile sensor and warhead technologies. A recent research effort [14, 15] focused on the development of integrated guidance-autopilot systems for a fixed-aim warhead missile. Integrated design techniques developed under these research efforts form the starting point for the present development of moving-mass guidance-autopilot system for KW.

The objective of the present research is to establish the feasibility of designing moving-mass actuated flight control systems for kinetic warheads that will meet the accuracy requirements in both exo-atmospheric and atmospheric target interception scenarios. This feasibility demonstration is achieved through a high-fidelity engagement simulation of a moving-mass controlled KW intercepting a tactical ballistic missile in various stages of flight.

Two different integrated guidance-autopilot systems based on the feedback linearization technique were synthesized using recently developed, computer-aided, nonlinear control system design software [16]. This software was developed under a previous research effort [17] with the Naval Surface Warfare Center, Dahlgren, VA. A unique feature of this software package is that it permits the direct synthesis of nonlinear control systems from simulation models of dynamic systems.

The following sections will discuss vehicle modeling, guidance-autopilot system design and evaluation in example engagement scenarios. Detailed modeling of a KW with moving-mass actuators will be given in Section 2. Flight control system designs and engagement simulation results will be presented Section 3. Conclusions from the present research will be given in Section 4.

2. Moving Mass Actuated Kinetic Warhead Model

This section will present the formulation of a 9 degree-of-freedom model of the kinetic warhead with moving-mass actuators. The equations of motion were coded in FORTRAN and then used in conjunction with Simulink® [18] to produce a simulation of the kinetic warhead.

2.1 Kinetic Warhead Model

In the present study, the kinetic warhead consists of a cone-shaped body with three actuator masses that can move parallel to the three orthogonal axes of the vehicle. A free-

body diagram of the kinetic warhead is shown in Figure 2.

In addition to the acceleration due to gravity, the kinetic warhead will experience aerodynamic forces in atmospheric flight. In exo-atmospheric flight, thrust is the dominant external force that acts on the vehicle.

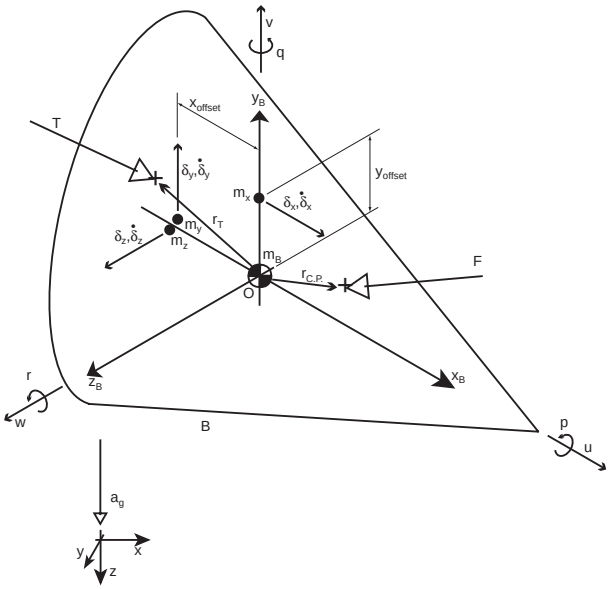

Figure 2. Kinetic Warhead

2.1.1 Nomenclature

The following notation is used in deriving the equations of motion (see Figure 2):

- m_B is the mass of the kinetic warhead body B.
- m_x, m_y, m_z are the actuator masses moving parallel to the body x, y, and z axes, respectively.
- m_T is the total mass of the kinetic warhead and the actuator masses
- $V_O = [u \;\; v \;\; w]'$ is the inertial velocity vector of the center of mass of the vehicle body B.
- $\omega_B = [p \;\; q \;\; r]'$ is the inertial angular velocity vector of the body B.
- $p_x = \begin{bmatrix} \delta_x \\ y_{offset} \\ 0 \end{bmatrix}$, $p_y = \begin{bmatrix} -x_{offset} \\ \delta_y \\ 0 \end{bmatrix}$,
- $p_z = \begin{bmatrix} -x_{offset} \\ 0 \\ \delta_z \end{bmatrix}$

  are the position vectors of the actuator masses in the body frame centered at the vehicle center of mass. The mass offsets x_{offset}, y_{offset} are assumed to be specified. The variables δ_x, δ_y, δ_z are the displacements of the three masses.
- $\dot{p}_x = \begin{bmatrix} \dot{\delta}_x \\ 0 \\ 0 \end{bmatrix}$, $\dot{p}_y = \begin{bmatrix} 0 \\ \dot{\delta}_y \\ 0 \end{bmatrix}$, $\dot{p}_z = \begin{bmatrix} 0 \\ 0 \\ \dot{\delta}_z \end{bmatrix}$

  are the relative velocities of the actuator masses with respect to the body B.
- $b_1^t = \begin{bmatrix} 1 \\ 0 \\ 0 \end{bmatrix}$, $b_2^t = \begin{bmatrix} 0 \\ 1 \\ 0 \end{bmatrix}$, $b_3^t = \begin{bmatrix} 0 \\ 0 \\ 1 \end{bmatrix}$

  are orthonormal basis vectors.
- u_x, u_y, u_z are the control forces acting on the x, y, and z axis actuator masses, respectively.
- $I_{B/O}$ is the 3×3 inertia matrix of the body B about its center of mass.
- r_{CP} is the position vector of the aerodynamic center of pressure from the center of mass of body B.
- r_T is the position vector of the point of application of the external thrust vector T from the center of mass of body B.
- F is the vector of aerodynamic forces at the center of pressure in the body frame.
- M is the vector of aerodynamic moments about the center of pressure in the body frame.
- T is the thrust vector in the body frame.
- $a_g = \begin{bmatrix} 0 \\ 0 \\ g \end{bmatrix}$ is the gravity vector in the

  inertial frame. The acceleration due to gravity is given by:

$g = 32.174\left(\frac{R_E}{R_E + h}\right)^2$ where h is altitude. $R_E = 2.0925\times10^7$ ft is the mean radius of the earth.

- C_{NB} is the transformation matrix from the body frame to the inertial frame.

The equations of motion of the kinetic warhead are derived using Kane's method [19]. The mathematical model consists of the dynamical and kinematical equations given in the two following subsections.

2.1.2 Dynamical Equations

The kinetic warhead translational dynamics are given by Equation (1).

$$\begin{aligned} & m_T\dot{V}_O - \left(m_x p_x + m_y p_y + m_z p_z\right)\times\dot{\omega}_B \\ & + m_x\ddot{p}_x + m_y\ddot{p}_y + m_z\ddot{p}_z \\ & = -\omega_B \times \left\{m_T V_O + m_x\left(\omega_B \times p_x + 2\dot{p}_x\right)\right. \\ & \left. + m_y\left(\omega_B \times p_y + 2\dot{p}_y\right) + m_z\left(\omega_B \times p_z + 2\dot{p}_z\right)\right\} \\ & + F + m_T C_{NB}^t a_g + T \end{aligned} \tag{1}$$

The vehicle rotational dynamics are given by Equation (2).

$$\begin{aligned} & \left(m_x p_x + m_y p_y + m_z p_z\right)\times\dot{V}_O + I_{B/O}\dot{\omega}_B \\ & - \left(m_x p_x \times p_x + m_y p_y \times p_y + m_z p_z \times p_z\right)\times\dot{\omega}_B \\ & + m_x p_x \times \ddot{p}_x + m_y p_y \times \ddot{p}_y + m_z p_z \times \ddot{p}_z \\ & = -\{\ \omega_B \times I_{B/O}\omega_B + m_x p_x \times \omega_B \times \left(V_O + \omega_B \times p_x + 2\dot{p}_x\right) \\ & + m_y p_y \times \omega_B \times \left(V_O + \omega_B \times p_y + 2\dot{p}_y\right) \\ & + m_z p_z \times \omega_B \times \left(V_O + \omega_B \times p_R + 2\dot{p}_z\right)\ \} \\ & + M + \left(r_{CP} \times F\right) + \left(r_{TH} \times T\right) \\ & + \left(m_x p_x + m_y p_y + m_z p_z\right)\times C_{NB}^t a_g \end{aligned} \tag{2}$$

The motions of the actuator masses are described by Equations (3) – (5).

$$\begin{aligned} & m_x b_1^t\left(\ \dot{V}_O - p_x \times \dot{\omega}_B\ \right) + m_x\ddot{\delta}_x \\ & = -m_x b_1^t\left[\omega_B \times \left(V_O + \omega_B \times p_x + 2\dot{p}_x\right) - C_{NB}^t a_g\right] \\ & + u_x \end{aligned} \tag{3}$$

$$\begin{aligned} & m_y b_2^t\left(\ \dot{V}_O - p_y \times \dot{\omega}_B\ \right) + m_y\ddot{\delta}_y \\ & = -m_y b_2^t\left[\omega_B \times \left(V_O + \omega_B \times p_y + 2\dot{p}_y\right) - C_{NB}^t a_g\right] \\ & + u_y \end{aligned} \tag{4}$$

$$\begin{aligned} & m_z b_3^t\left(\ \dot{V}_O - p_z \times \dot{\omega}_B\ \right) + m_z\ddot{\delta}_z \\ & = -m_z b_3^t\left[\omega_B \times \left(V_O + \omega_B \times p_z + 2\dot{p}_z\right) - C_{NB}^t a_g\right] \\ & + u_z \end{aligned} \tag{5}$$

At each value of the state vector, the nine dynamical equations in (1) – (5) can be solved as a system of linear equations to obtain the state rates of the system dynamics:

$$A(x)\begin{bmatrix} \dot{V}_O \\ \dot{\omega}_B \\ \ddot{\delta}_x \\ \ddot{\delta}_y \\ \ddot{\delta}_z \end{bmatrix} = f(x,u)$$ where x is the state vector and $A(x)$ is a 9x9 matrix.

These state rates are used in conjunction with numerical integration algorithms to generate temporal histories of the state variables. The dynamical equations have to be augmented with the kinematical equations given in the next section to complete the description of the kinetic warhead dynamics.

2.1.3 Kinematical Equations

The inertial-frame position of the mass center of the vehicle body B is given by Equation (6).

$$\begin{aligned} \begin{pmatrix} \dot{x} \\ \dot{y} \\ \dot{z} \end{pmatrix} &= \begin{bmatrix} 1-2(q_2^2+q_3^2) & 2(q_1q_2 - q_3q_4) & 2(q_1q_3 + q_2q_4) \\ 2(q_1q_2 + q_3q_4) & 1-2(q_1^2+q_3^2) & 2(q_2q_3 - q_1q_4) \\ 2(q_1q_3 - q_2q_4) & 2(q_2q_3 + q_1q_4) & 1-2(q_1^2+q_2^2) \end{bmatrix}(V_O) \\ &= C_{NB}V_O \end{aligned} \tag{6}$$

where $q_1 - q_4$ are the Euler parameters or quaternions.

The temporal evolution of the quaternions is governed by the differential equation (7):

$$\begin{pmatrix} \dot{q}_1 \\ \dot{q}_2 \\ \dot{q}_3 \\ \dot{q}_4 \end{pmatrix} = 0.5 \begin{bmatrix} q_4 & -q_3 & q_2 \\ q_3 & q_4 & -q_1 \\ -q_2 & q_1 & q_4 \\ -q_1 & -q_2 & -q_3 \end{bmatrix} (\omega_B) \qquad (7)$$

2.1.4 Kinetic Warhead Properties

The values of the various physical properties of the kinetic warhead are as follows. These were obtained from Reference 3:

m_B = 55 lbm = 1.7095 slugs

$m_x = m_y = m_z$ = 5 lbm. = 0.1554 slugs

$$I_{B/O} = \begin{bmatrix} 0.12821 & 0 & 0 \\ 0 & 0.6 & 0 \\ 0 & 0 & 0.6 \end{bmatrix} \text{slug-ft}^2,$$

where the I_{11} term was computed assuming a solid right circular cone with a base diameter d = 1 ft, and I_{22} and I_{33} are from Reference 3.

The thrust vector T used for exo-atmospheric engagements was $[500 \ 0 \ 0]^T$ lbf.

2.1.5 Aerodynamic Model

The normal and axial forces due to aerodynamics are computed using the expressions:

$$F_N = \bar{Q} S_{ref} C_N, \quad F_x = -\bar{Q} S_{ref} C_A,$$
$$\bar{Q} = \tfrac{1}{2} \rho V^2, \quad S_{ref} = \pi d^2 / 4 = (\pi / 4) \qquad (8)$$

where the coefficients C_N and C_A are interpolated from tabular data provided by the Navy [20], and V is the total velocity, the magnitude of the inertial velocity vector whose body-axis components are u, v, and w. The aerodynamic coefficients are specified as functions of Mach number and the total angle of attack α_T

$$\alpha_T = \cos^{-1}\left(\frac{u}{V}\right) \qquad (9)$$

The axial and normal force coefficients plotted in Figure 3 and Figure 4 illustrate the nature of their dependence on Mach number and the total angle of attack. The normal force F_N is resolved into the body-axis y and z components as:

$$F_y = \frac{v}{\sqrt{v^2 + w^2}} F_N, \quad F_z = \frac{w}{\sqrt{v^2 + w^2}} F_N \qquad (10)$$

Aerodynamic moment coefficients were not available at the time of this study. Hence, the aerodynamic moments are computed using the lift and drag forces acting at the aerodynamic center, with the static margin as the lever arm. The static margin was set to 0.01 ft for all the simulations given in this paper. The location of the aerodynamic center is assumed to be independent of Mach number and total angle of attack. Aerodynamic damping and unsteady aerodynamic effects are neglected.

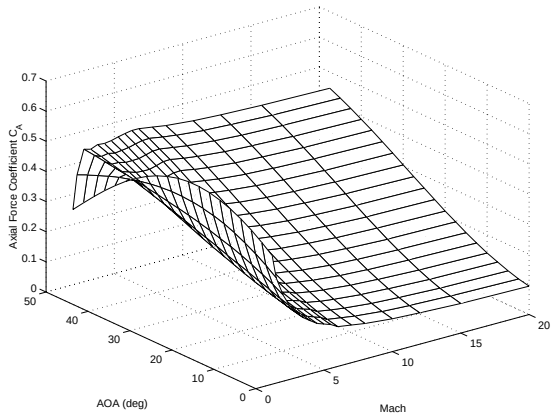

Figure 3. Axial Force Coefficient vs. Angle of Attack and Mach Number

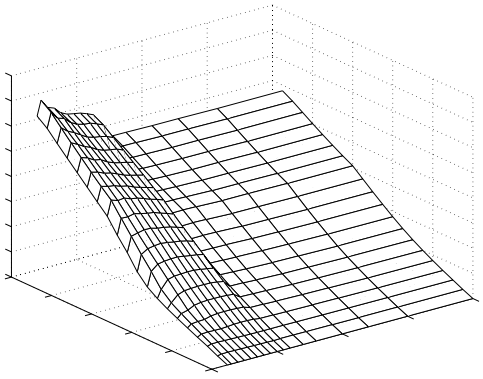

Figure 4. Normal Force Coefficient vs. Angle of Attack and Mach Number

Atmospheric density and the speed of sound were computed using the 1976 U.S. standard atmosphere model. In the present study, the atmospheric model is defined for altitudes up to 435 miles, although aerodynamic effects are expected to be insignificant above about 37 miles.

2.1.6 Moving-Mass Positioning Actuator Model

The moving masses are assumed to be positioned by proportional plus derivative servos. The servo gains are chosen to yield an undamped natural frequency of 50 Hz, with 0.71 damping ratio. In response to a commanded displacement of δ_{ic} the actuator servo will apply a force

$$F_i = -k_p\left(\delta_i - \delta_{ic}\right) - k_d\dot{\delta}_i \qquad (11)$$

on the moving mass. The proportional gain k_p (lbf/ft) and the derivative gain k_d (lbf/ft/s) corresponding to actuator natural frequency and damping, can be computed as 15340 and 70, respectively. Note that these gains correspond to a moving mass of 0.1554 slugs (5 lb).

The displacements of the actuator masses are limited since the mass cannot travel beyond the confines of the vehicle. These constraints are enforced by adding constraint forces to the equations of motion so as to bring the velocity of the moving masses to zero when the displacement approaches its limit and to counter the actuator force as long as it pushes the mass against the stop. Moreover, limits were also imposed on the control forces applied by the servos.

2.1.7 Line-of-Sight Angles and Rates

In addition to the equations of motion, the guidance law computations often require the line-of –sight angles and rates. The definition of line-of-sight (LOS) angles λ_y, λ_z are illustrated in Figure 5.

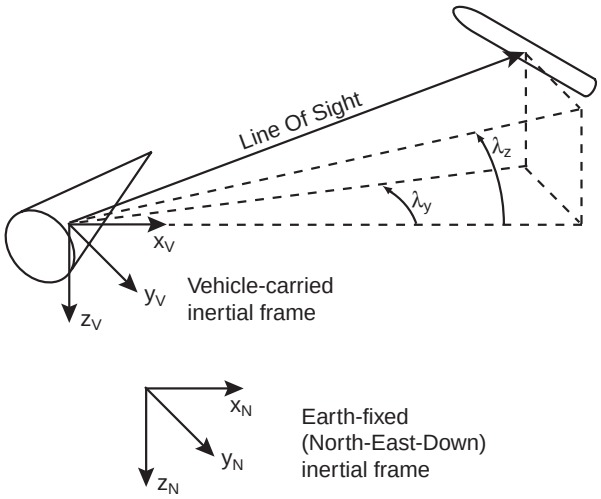

Figure 5. Line Of Sight Angles

The missile relative-target position vector, or the line-of-sight, in the inertial frame is

$$\vec{r} = \vec{r}_t - \vec{r}_{kw} \qquad (12)$$

where $\vec{r}_t = \begin{bmatrix} x_t & y_t & z_t \end{bmatrix}^t$ and $\vec{r}_{kw} = \begin{bmatrix} x_{kw} & y_{kw} & z_{kw} \end{bmatrix}^t$ are the inertial position vectors of the target and the kinetic warhead, respectively. Let $\vec{r} = \begin{bmatrix} r_x & r_y & r_z \end{bmatrix}^t$. The line-of-sight angles can then be defined as:

$$\lambda_y = tan^{-1}\left(\frac{r_y}{r_x}\right), \lambda_z = tan^{-1}\left(\frac{r_z}{r_x}\right) \qquad (13)$$

The difference between the inertial velocity vectors, expressed in the Earth-fixed inertial frame, is the relative velocity, represented by $\dot{\vec{r}} = \begin{bmatrix} \dot{r}_x & \dot{r}_y & \dot{r}_z \end{bmatrix}^T = V_t - C_{NB}V_O$. The line-of-sight angular rates are obtained by taking the time derivatives of the LOS angles above:

$$\dot{\lambda}_y = \frac{\dot{r}_y - \dot{r}_x\, tan\,\lambda_y}{r_x\, sec^2\,\lambda_y} = \frac{r_x\dot{r}_y - \dot{r}_x r_y}{r^2},$$

$$\dot{\lambda}_z = \frac{\dot{r}_z - \dot{r}_x\, tan\,\lambda_z}{r_x\, sec^2\,\lambda_z} = \frac{r_x\dot{r}_z - \dot{r}_x r_z}{r^2} \qquad (14)$$

where $r = \left(r_x^2 + r_y^2 + r_z^2\right)^{1/2}$.

The expressions for angular acceleration of the LOS angle required in one of the integrated flight control system designs can be computed from the following geometric relationships.

$$\ddot{\lambda}_y = \frac{r\left(r_x \ddot{r}_y - \ddot{r}_x r_y\right) - 2\dot{r}\left(r_x \dot{r}_y - \dot{r}_x r_y\right)}{r^3},$$

$$\ddot{\lambda}_z = \frac{r\left(r_x \ddot{r}_z - \ddot{r}_x r_z\right) - 2\dot{r}\left(r_x \dot{r}_z - \dot{r}_x r_z\right)}{r^3} \qquad (15)$$

where the relative inertial acceleration is $\ddot{\vec{r}} = \left[\ddot{r}_x \quad \ddot{r}_y \quad \ddot{r}_z\right]^t = a_t - a_{kw}$. The inertial acceleration of the kinetic warhead is $a_{kw} = C_{NB}\left(\dot{V}_O + \omega \times V_O\right)$, and the acceleration of the target a_t is generally unknown, and needs to be estimated.

2.2 Target Model

A non-maneuvering target and a weaving target model are considered in the present research. The accelerations of the target in the inertial frame are:

$$\ddot{x} = 0, \quad \ddot{y} = 0, \quad \ddot{z} = g \quad OR \quad \ddot{z} = A\,\omega^2 \sin \omega t \qquad (16)$$

As can be garnered from the Equation (16), the nonmaneuvering target is assumed to be falling under the action of gravity. The weaving target model is assumed to be capable of 3 g normal acceleration with a frequency of 0.5 Hz.

3. Guidance and Control System Design

The dynamic model of the kinetic warhead described in Section 2 is used to develop control and guidance laws. This section will present the design of guidance and control laws for atmospheric and exo-atmospheric interception scenarios. The feedback linearization technique [9 – 13] is used to design nonlinear control laws using the complete model of the kinetic warhead. The feedback linearization methodology transforms a given nonlinear dynamic model into a linear, time-invariant form. Any linear control methodology can then be used to design the control system. Inverse transformation of the control law to the original coordinates then yields the nonlinear control law. The results given in this paper were obtained using the pole placement design technique in conjunction with the feedback linearization approach. A software package for feedback linearization developed under a previous research effort with the Navy [17] is used in the design process.

The following sections will discuss two different integrated flight control system designs. The integrated design methodology simultaneously addresses the guidance and autopilot design problems. An advantage of the integrated design methodology is that it eliminates the iterations between guidance and autopilot design processes required for satisfying the flight control system performance objectives. Detailed discussions on the benefits of the integrated design methodology are given in References 4, 5, 14, 15, 21 and 22.

3.1 Integrated Design Based on Line-of-Sight Rate Regulation

This integrated design approach is based on the proportional navigation concept, in the sense that the flight control system is designed with the objective of driving the line-of-sight rates to zero. The integrated guidance-autopilot system is also responsible for stabilizing the kinetic warhead dynamics. In order to design the integrated flight control system using the Nonlinear Synthesis Tools [16] software package, the control influence chain can be defined as:

$$u_z \rightarrow \dot{\delta}_z \rightarrow \delta_z \rightarrow q \rightarrow w \rightarrow \dot{\lambda}_z \qquad (17)$$

$$u_y \rightarrow \dot{\delta}_y \rightarrow \delta_y \rightarrow r \rightarrow v \rightarrow \dot{\lambda}_y \qquad (18)$$

These relationships describe the interdependence of control and state variables in the kinetic warhead dynamics. For instance, the first expression suggests that the force u_z acting on the moving mass influences the velocity $\dot{\delta}_z$ and position δ_z of the moving mass along the z-axis, which in turn influences the kinetic warhead pitch rate q resulting in a change in the body velocity component w along the z-axis. This velocity component will result in an acceleration component normal to the kinetic warhead, which will then influence the line-of-sight rate $\dot{\lambda}_z$. A similar

description can be also be generated for Expression (18).

The control influence chains are provided to the nonlinear control system design software in the form of a matrix, Reference 16 gives additional details on how this matrix can be formulated in a given problem.

3.1.1 Engagement Scenario 1

The first engagement scenario used to evaluate the integrated guidance-autopilot system is described below. The closed-loop poles in both channels were {-51, -50, -35, -30, -20}. The kinetic warhead and target trajectories are shown in Figure 6 and Figure 7.

This engagement scenario is similar to the endo-atmospheric engagement considered in Reference 3 in which both the warhead and target are initially at an altitude of 45,000 ft, and 50,000 ft. apart. Both vehicles have 15-degree flight path angles and are on reciprocal headings, and both have an initial velocity of 6000 ft/sec. In addition, the target has an initial offset of 1000 ft. in the east direction.

The miss distance for this engagement was 0.28 ft. The line of sight rates are shown in Figure 8. The integrated guidance-autopilot drives the line-of-sight rates to near-zero early in the engagement, and then attempts to keep it there. Note that it is possible to introduce dynamic compensation networks in the integrated guidance-autopilot to distribute the control effort more uniformly over the engagement. Moreover, the gain in the line-of-sight rate states can be increased to further reduce the miss distance.

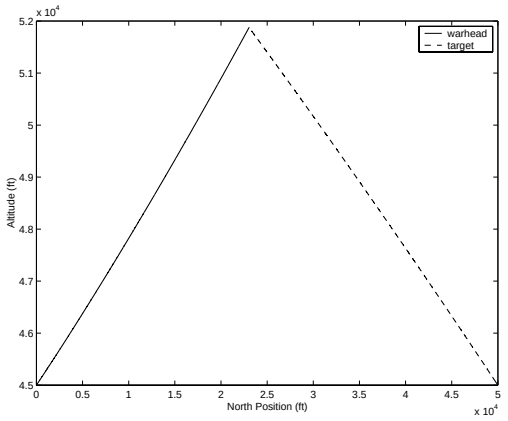

Figure 6. Warhead and Target Trajectories, Vertical Plane

The angle of attack and angle of sideslip are shown in Figure 9. There is a large initial acceleration seen in Figure 10, particularly in the lateral channel, to remove the LOS error. A noticeable roll rate is induced due to the moving masses, which can be seen in the angular velocities shown in Figure 11. The actuator mass displacements and the control forces are shown in Figure 12.

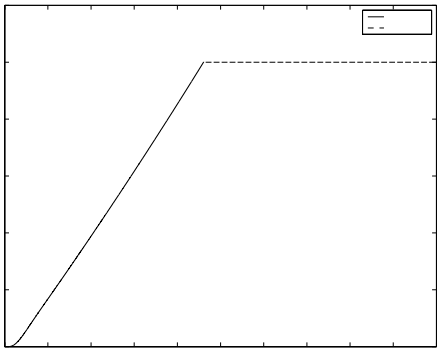

Figure 7. Warhead and Target Trajectories, Horizontal Plane

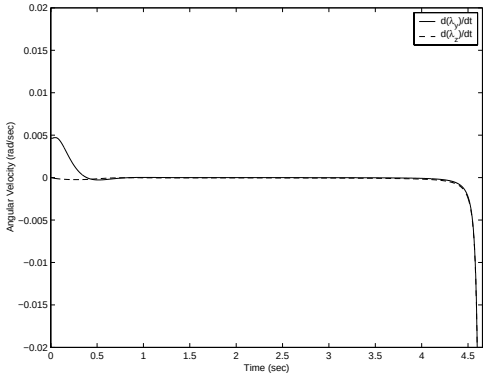

Figure 8. Line Of Sight Rates vs. Time

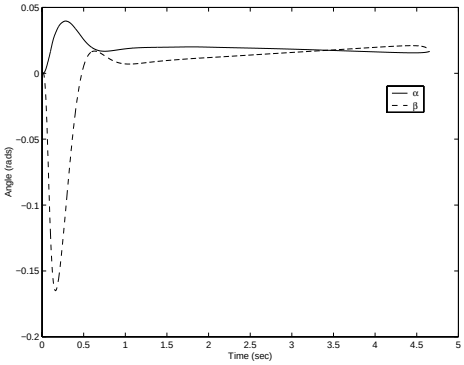

Figure 9. Angles of Attack and Sideslip vs. Time

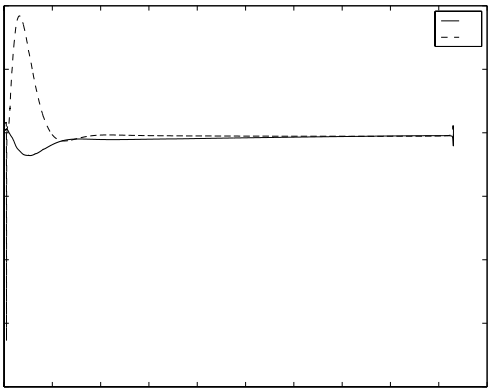

Figure 10. Body-Frame Accelerations vs. Time

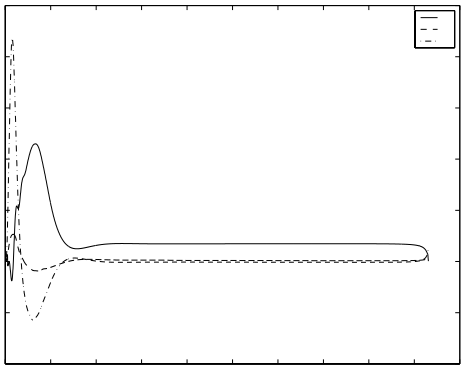

Figure 11. Body Angular Velocities vs. Time

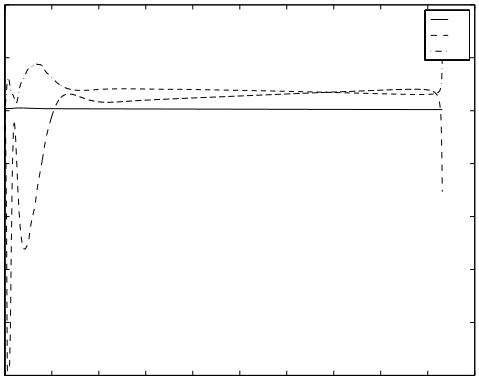

Figure 12. Actuator Mass Displacements vs. Time

3.1.2 Engagement Scenario 2

The second scenario is the exo-atmospheric case from Reference 3 where the warhead and target start at an altitude of 545,000 ft. and are 120,000 ft. apart on reciprocal headings and flight path angles of 45 degrees. Both vehicles have an initial velocity of 6000 ft/sec. In this case the poles had to be slowed down due to the smaller force available for steering. The closed loop poles were {-51, -50, -25, -20, -10} in both channels. The kinetic warhead and target trajectories are shown in Figure 13. The miss distance was 0.42 ft.

The line of sight rates are shown in Figure 14. As in the previous engagement scenario, the integrated guidance-autopilot system proceeds

to correct most of the line-of-sight rates at the beginning of the engagement. The angle of attack and angle of sideslip are shown in Figure 15. The accelerations are seen in Figure 16. The accelerations shown are in the wind frame, i.e. perpendicular to the velocity vector, instead of the body frame as was shown in the atmospheric case. This is because of the fact that since the maneuvering forces are derived primarily from the thrust vector acting along the kinetic warhead longitudinal axis, acceleration components normal to the velocity vector can be nonzero, while the lateral and normal acceleration components along the body axes remain near zero.

As in the atmospheric interception scenario, there is a large increase in acceleration at the beginning of the engagement. Note that since the thrust is 500 lbf and the total mass is 70 lbm, the maximum acceleration obtainable is around 7 g's. Figure 15 shows that the maximum angle of attack during the engagement was about 68 degrees. Note that this fact has important bearing on the types of seekers that can be employed in conjunction with the moving mass control of kinetic warheads. Engagements can be accomplished with smaller angle of attack and angle of sideslip if higher thrust levels are available. The angular velocities and quaternions are shown in Figure 17. The actuator mass displacements and the control forces are shown in Figure 18.

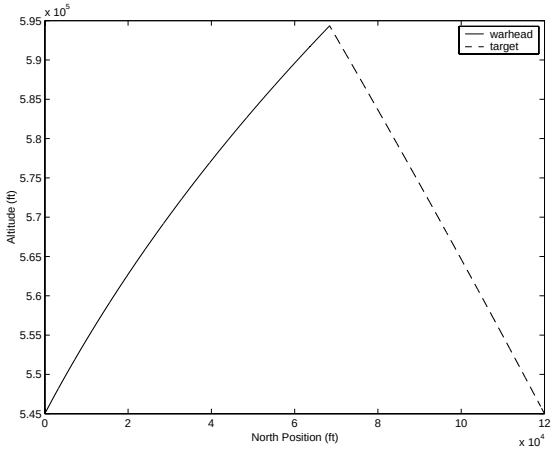

Figure 13. Warhead and Target Trajectories, Vertical Plane

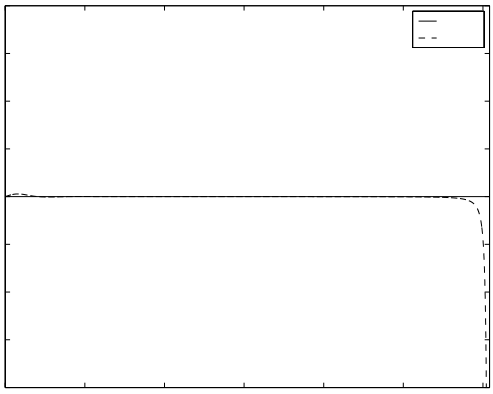

Figure 14. Line of Sight Rates vs. Time

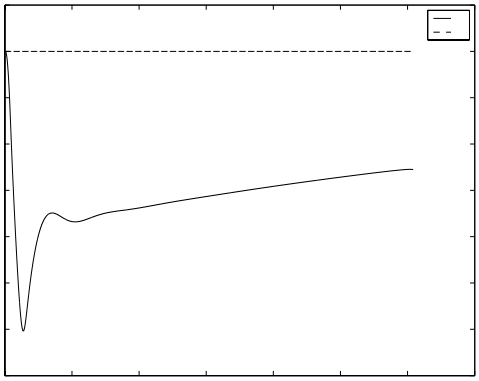

Figure 15. Angles of Attack and Sideslip vs. Time

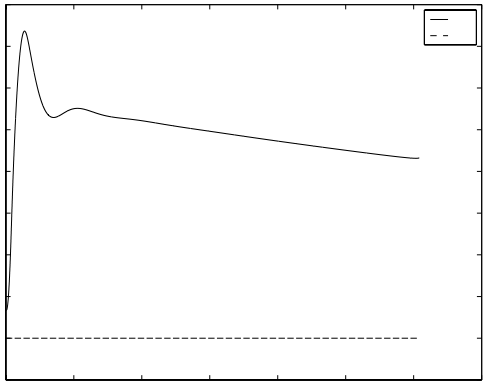

Figure 16. Wind-Frame Accelerations vs. Time

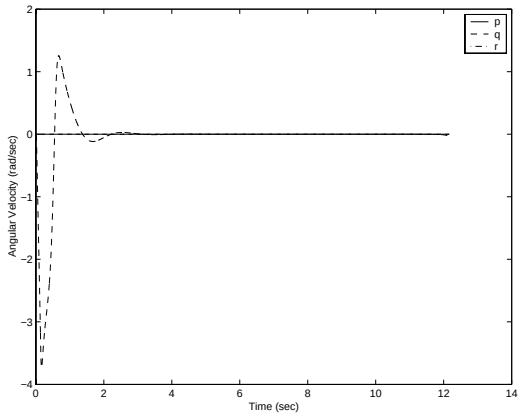

Figure 17. Body Angular Velocities vs. Time

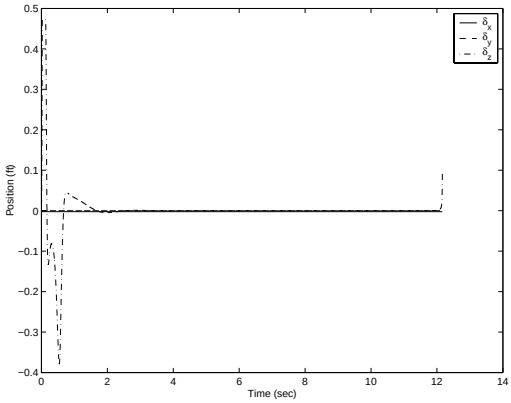

Figure 18. Actuator Mass Displacements vs. Time

3.1.3 Engagement Scenario 3

This engagement features a weaving target example from Reference 3. The warhead and target are initially at an altitude of 45,000 ft. and are headed directly toward each other. The initial velocities are 6000 ft/sec. for both vehicles. The target weaves in the vertical plane with an acceleration of 3 g and a frequency of 0.5 Hz. The poles of the integrated flight control system were chosen to be the same as in Subsection 3.2.1.

The kinetic warhead and target trajectories are shown in Figure 19. The terminal miss distance for this case was 0.28 ft. The line of sight rates are shown in Figure 20. As in the previous engagement scenarios, the flight control system attempts to maintain the line-of-sight rates close to zero. However, the flight control system encounters difficulties in maintaining these quantities close to zero due to the dynamic nature of the target. The angle of attack and angle of sideslip are shown in Figure 21. The actuator mass displacements and the control forces are shown in Figure 22.

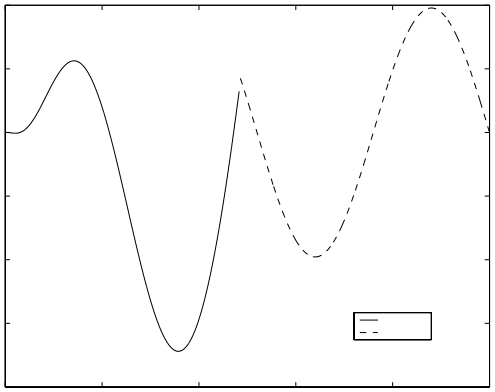

Figure 19. Warhead and Target Trajectories, Vertical Plane

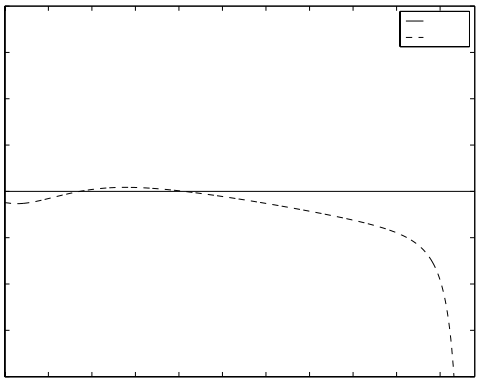

Figure 20. Line of Sight Rates vs. Time

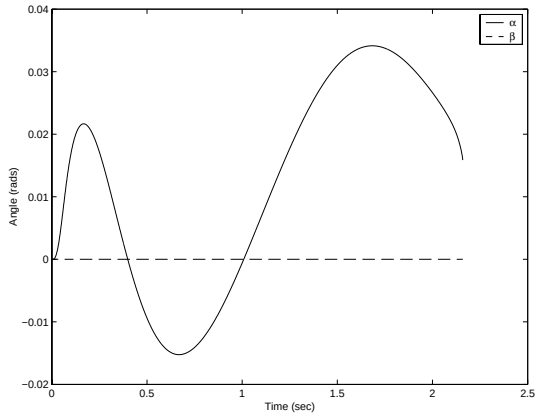

Figure 21. Angles of Attack and Sideslip vs. Time

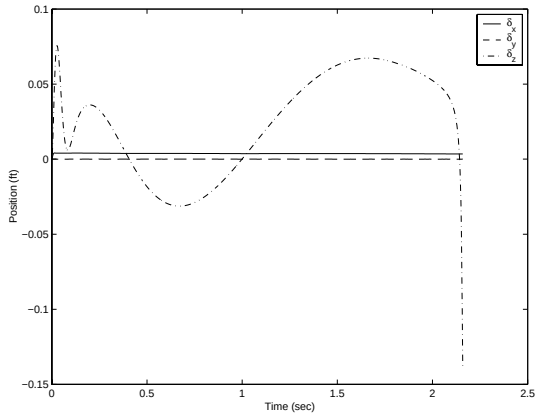

Figure 22. Actuator Mass Displacements vs. Time

3.2 Integrated Design Based on Collision Course Tracking

The second version of the integrated flight control system design continuously attempts to align the kinetic warhead velocity vector along the collision course with the target. This is accomplished by constructing a tracking system for the flight path and heading angle commands and a command generator that computes the necessary angles to achieve a collision. The flight path angle (γ) and the heading angle (χ) are defined as:

$$\gamma = -tan^{-1}\left(\frac{\dot{z}}{\sqrt{\dot{x}^2+\dot{y}^2}}\right), \quad \chi = tan^{-1}\left(\frac{\dot{y}}{\dot{x}}\right) \tag{19}$$

where $[\dot{x} \quad \dot{y} \quad \dot{z}]^t = C_{NB}V_O$ are the kinetic warhead velocity components expressed in the inertial frame. The errors between the actual and desired angles are integrated with time, and these integrator states are also fed back. The control influence chains for the integrated control system design are:

$$u_z \rightarrow \dot{\delta}_z \rightarrow \delta_z \rightarrow q \rightarrow w \rightarrow \gamma \rightarrow \int[\gamma_c - \gamma]dt \tag{20}$$

$$u_y \rightarrow \dot{\delta}_y \rightarrow \delta_y \rightarrow r \rightarrow v \rightarrow \chi \rightarrow \int[\chi_c - \chi]dt \tag{21}$$

The collision course is computed by assuming that the target and warhead fly at constant speeds and directions until collision at time t_{go}. The kinetic warhead velocity components required to achieve interception can be computed from the collision conditions. For instance, along the *x*-direction in the inertial frame, the collision conditions require:

$$\begin{aligned} &x_{kw}(0) + t_{go}\dot{x}_{kw} = x_{kw}(t_{go}) \\ &= x_t(t_{go}) = x_t(0) + t_{go}\dot{x}_t \end{aligned} \tag{22}$$

This expression can be simplified to yield:

$$\dot{x}_{kw} = \frac{x_t(0) - x_{kw}(0)}{t_{go}} + \dot{x}_t \tag{23}$$

The kinetic warhead velocity vector components along the *y* and *z* directions can be computed similarly. If information about the target acceleration is available it can be included in the above equation. The time-to-go is estimated from the range and range rate:

$$t_{go} = -\frac{r}{\dot{r}} \tag{24}$$

The differential equations for flight path and heading angles needed for the computation of the control law are given by:

$$\dot{\gamma} = \frac{(\dot{x}\ddot{x} + \dot{y}\ddot{y})\dot{z} - (\dot{x}^2 + \dot{y}^2)\ddot{z}}{\sqrt{\dot{x}^2+\dot{y}^2}(\dot{x}^2+\dot{y}^2+\dot{z}^2)}, \quad \dot{\chi} = \frac{(\dot{x}\ddot{y} - \ddot{x}\dot{y})}{(\dot{x}^2+\dot{y}^2)} \tag{25}$$

The control chains defined in Expressions (20) and (21), together with the expressions for command generation and the expressions for flight path angle and heading angle are used in conjunction with the Nonlinear Synthesis Tools [16] software package to derive the integrated flight control system. The performance of this integrated guidance-autopilot is then assessed for an engagement scenario defined in the following subsection.

3.2.1 Engagement Scenario 1

In this engagement scenario, both the warhead and target are initially at an altitude of 45,000 ft, and 50,000 ft apart. Both vehicles have 15-degree flight path angles and are on reciprocal headings, and both have an initial velocity of 6000 ft/sec. In addition, the target has an initial offset of 1000 ft. in the east direction.

The closed-loop poles were chosen to be {-99, -90, -35, -30, -6, -1} in both channels. Trajectories are shown in Figure 23 and Figure 24. The terminal miss distance was 0.027 ft. The line-of-sight rates are shown in Figure 25. It may be observed that the line-of-sight rate corrections are a little more distributed over the engagement than in the integrated flight control system discussed in Section 3.2.1. The angle of attack and angle of sideslip are shown in Figure 26. There is a large initial acceleration seen in Figure 27 in the lateral channel to eliminate the offset. The longitudinal channel maintains some acceleration throughout the flight. A noticeable roll rate is induced which can be seen in the angular velocities shown in Figure 28. The actuator mass displacements and the control forces are shown in Figure 29. As in the previous designs, the force requirements are well within the capabilities of commercial off-the-shelf linear electric motors.

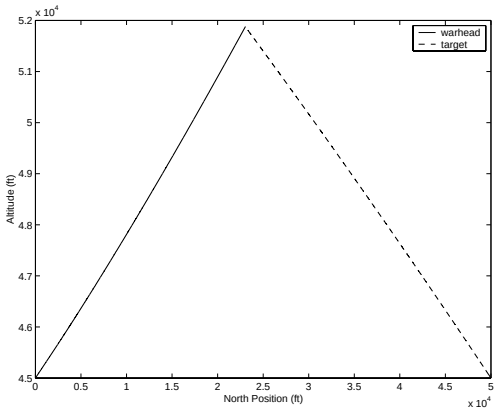

Figure 23. Warhead and Target Trajectories, Vertical Plane

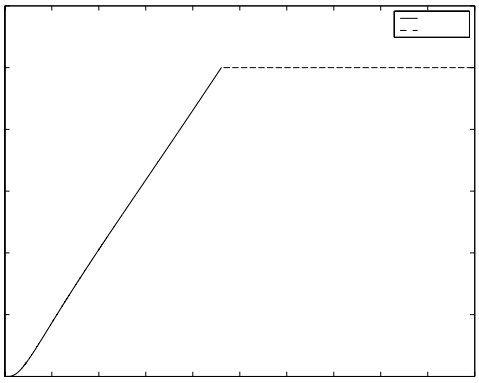

Figure 24. Warhead and Target Trajectories, Horizontal Plane

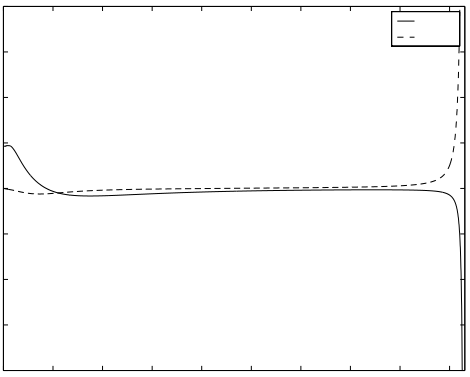

Figure 25. Line Of Sight Rates vs. Time

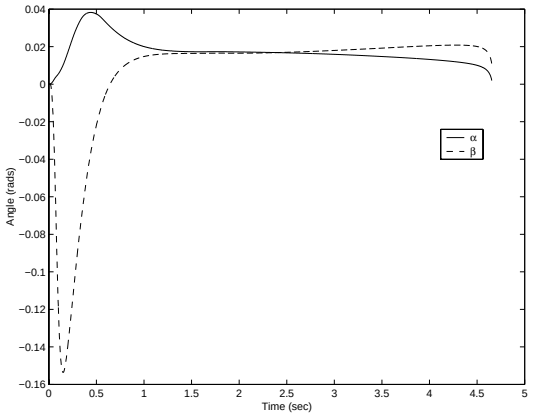

Figure 26. Angles of Attack and Sideslip vs. Time

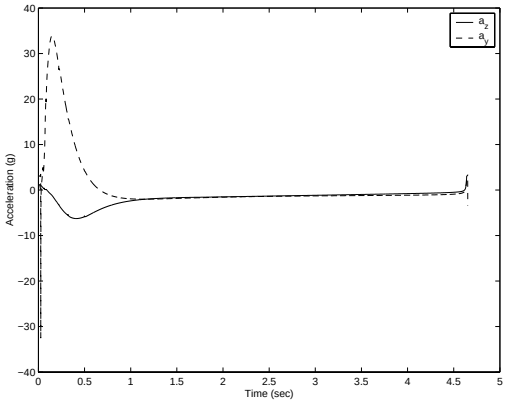

Figure 27. Body-Frame Inertial Accelerations vs. Time

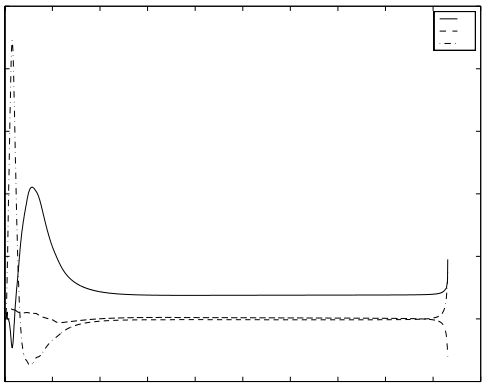

Figure 28. Body Angular Velocities vs. Time

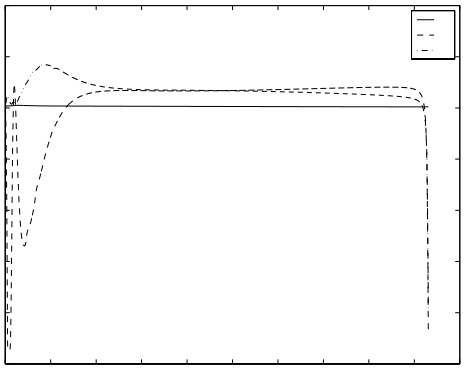

Figure 29. Actuator Mass Displacements vs. Time

The engagement results given in these sections demonstrate the feasibility of using the moving mass actuation concept for the kinetic warhead. Note that the miss distances obtained in this preliminary work can be significantly improved by introducing additional dynamic compensation in the guidance-autopilot loop. It is important to state here that the present results were obtained without including various error sources in the guidance-autopilot loop. Future work will examine the performance of the integrated guidance-autopilot system in the presence of disturbances and sensor errors, and will investigate approaches for making the system robust with respect to target maneuvers and other disturbances. The present research shows that integrated guidance-autopilot system design methodology is an effective and flexible flight control system design method.

A survey of electric actuators were conducted during the present research. Preliminary analysis indicates that the moving-mass control concept can be realized using readily available, commercial, off-the-shelf linear electric motor technology.

4. Conclusions and Future Work

This paper described the modeling, simulation, and integrated guidance and control of a kinetic warhead utilizing moving-mass actuators. Moving mass actuation methodology can be used in any speed range both in the

atmosphere as well as outside it, as long as there is a force, either aerodynamic or propulsive, acting on the vehicle. Since they are contained entirely within the airframe geometric envelope, and because no mass expulsion is involved, moving-mass actuation technique offers several advantages over conventional aerodynamic control surfaces and reaction control systems. The disadvantages of the moving mass actuation technology are that the airframe must provide adequate internal space for the moving masses, and must have near-neutral aerodynamic static stability characteristics.

The present work has developed a high fidelity, 9 degree-of-freedom simulation model of a kinetic warhead with three moving-mass actuators. This simulation model was used for actuator sizing and in the development of flight control systems. Commercial, off-the-shelf linear electric motors appear to be capable of providing the necessary force and speed of response characteristics for positioning the moving masses within the airframe.

A software package for performing numerical feedback linearization technique developed under a previous research effort was used to design nonlinear flight control systems. Pole placement technique was then used to design the feedback linearized flight control system. Two different integrated design methodologies were illustrated, the first based on regulating the line-of-sight rates, and the second one controlling the trajectory about the collision course. Interception of non-maneuvering and weaving targets in both atmospheric and exo-atmospheric conditions were illustrated. In every case, the moving mass integrated guidance-autopilot was able to deliver a miss distance smaller than half the diameter of the kinetic warhead. Additional improvements in the guidance-autopilot system design are feasible through the introduction of dynamic compensators in the flight control loop.

Future research will examine the impact of uncertainties in the target maneuvers and environmental factors on the kinetic warhead performance. Application of the moving mass control technology to other flight vehicles and underwater vehicles will also be of future interest.

Acknowledgement

This research was conducted under Navy Contract No. N00178-01-C-1020. The authors would like to thank Dr. Pashang Esfandiari (PMS 452) for his interest and support of this work.

References

[1] Chanute, O., *Progress in Flying Machines*, Dover, Mineola, NY, 1997.

[2] Wolko, H. S. (Editor), *The Wright Flyer*, Smithsonian Institution Press, Washington, D. C., 1987.

[3] Chadwick, W. R., and Malyevac, D. S., "Considerations on the Design of Kinetic Kill Interceptor with Moving Mass Control", Draft Report NSWCDD TR-00/87, Naval Surface Warfare Center, Dahlgren, VA, August, 2000.

[4] Menon, P. K. and Iragavarapu, V. R., "Integrated Design of Agile Missile Guidance and Control Systems", Final Report Submitted under Navy Contract No. N00178-97-C-1028, Optimal Synthesis Inc., Palo Alto, CA, October 1998.

[5] Menon, P. K., Iragavarapu, V. R., and Ohlmeyer, E. J., "Integrated Design of Agile Missile Guidance and Control System", *AIAA Missile Sciences Conference*, November 17-19, 1998, Monterey, CA.

[6] Cloutier, J. R., D'Souza, C. N., and Mracek, C. P., "Nonlinear Regulation and Nonlinear H∞ Control Via the State-Dependent Riccati Equation Technique", Proceedings of the *International Conference on Nonlinear Problems in Aviation and Aerospace*, Daytona Beach, FL, May, 1996.

[7] Mracek, C.P. and Cloutier, J. R., "Full Envelope Missile Longitudinal Autopilot Design using the State-Dependent Riccati Equation Method", Proceedings of the

AIAA Guidance, Navigation and Control Conference, August 11-13, 1997, New Orleans, LA, pp. 1697-1705.

[8] Cloutier, J. R., "State-Dependent Riccati Equation Techniques: An Overview", Proceedings of the *1997 American Control Conference*, June 4 - 6, Albuquerque, NM, pp. 932-936.

[9] Isidori, A., *Nonlinear Control Systems - An Introduction*, Springer-Verlag, New York, 1989.

[10] Marino, R., and Tomei, P., *Nonlinear Control Design*, Prentice Hall, New York, NY, 1995.

[11] Menon, P. K., Badgett, M. E., Walker, R. A., and Duke, E. L., "Nonlinear Flight Test Trajectory Controllers for Aircraft", *Journal of Guidance, Control, and Dynamics*, Vol. 10, Jan.-Feb. 1987, pp. 67-72.

[12] Lane, S. H., and Stengel, R. F., "Flight Control Design Using Nonlinear Inverse Dynamics", *Automatica*, Vol. 24, No. 4, 1988, pp. 471-483.

[13] Meyer, G., and Cicolani, L., "Application of Nonlinear Systems Inverses to Automatic Flight Control Design System Concepts and Flight Evaluation," *Theory and Applications of Optimal Control in Aerospace Systems*, AGARDograph 251, P. Kant (Editor), July 1981.

[14] Menon, P. K. and Ohlmeyer, E. J., "Integrated Design of Agile Missile Guidance and Autopilot Systems", IFAC Journal of *Control Engineering Practice*, Vol. 9, 2001, pp. 1095-1106.

[15] Menon, P. K., and Ohlmeyer, E. J., "Integrated Guidance-Control Systems for Fixed-Aim Warhead Missiles", *AIAA Missile Sciences Conference*, November 7-9, 2000, Monterey, CA.

[16] Menon, P. K., et al., *Nonlinear Synthesis Tools™ for Use with MATLAB®*, *Optimal Synthesis Inc.*, 2000, Palo Alto, CA.

[17] Menon, P. K., and Iragavarapu, V. R., "Robust Nonlinear Control Technology for High-Agility Missile Interceptors", Final Report Submitted under Navy Contract No. N00024-97-C-14178, *Optimal Synthesis Inc.*, Los Altos, CA, August 2000.

[18] Anon., *Using Simulink*, The MathWorks, Inc., Natick, MA, 2000.

[19] Kane, T. R. and Levinson, D. A., *Dynamics: Theory and Applications*, McGraw-Hill, New York, NY, 1985.

[20] Ohlmeyer, E. J., Electronic mail on Kinetic Warhead Aerodynamic Model, August 20, 2001.

[21] Palumbo, N. F., and Jackson, T. D., "Integrated Missile Guidance and Control: A State Dependent Riccati Differential Equation Approach", 1999 *IEEE International Conference on Control Applications*, August 22-27, Kohala Coast, Hawai'i, pp. 243-248.

[22] Menon, P. K., Dewell, L. D., and Sweriduk, G. D., "Integrated Guidance-Autopilot Designs for Anti-Jam Operation of Precision Munitions", Final Report prepared under Air Force Contract No. F08630-99-C-0040, *Optimal Synthesis Inc.*, Palo Alto, CA, January 2000.